Journal of Biomedical Optics

BiomedicalOptics.SPIEDigitalLibrary.org

Review of recent developments in stimulated emission depletion microscopy: applications on cell imaging

Bhanu Neupane
Frances S. Ligler
Gufeng Wang

SPIE.

Journal of Biomedical Optics 19(8), 080901 (August 2014)

REVIEW

Review of recent developments in stimulated emission depletion microscopy: applications on cell imaging

Bhanu Neupane,[a] Frances S. Ligler,[a,*] and Gufeng Wang[b,*]
[a]University of North Carolina at Chapel Hill and North Carolina State University, Department of Biomedical Engineering, Raleigh, North Carolina 27599-7115, United States
[b]North Carolina State University, Department of Chemistry, Raleigh, North Carolina 27695-8204, United States

Abstract. Stimulated emission depletion (STED) microscopy is one type of far-field optical technique demonstrated to provide subdiffraction resolution. STED microscopy utilizes a donut-shaped depletion beam to limit the probe volume to be much smaller than a diffraction-limited spot. Resolutions as small as a few tens of nanometers laterally are reported for cell analysis. The different versions of STED microscopes are described and contrasted in terms of their applicability for biological imaging. Finally, we suggest likely avenues for improving the performance and increasing the utility of STED microscopy. [DOI: 10.1117/1.JBO.19.8.080901]

Keywords: STED; optical resolution; diffraction limit; live cell imaging.

Paper 140300VR received May 13, 2014; revised manuscript received Jul. 18, 2014; accepted for publication Jul. 21, 2014; published online Aug. 14, 2014.

1 Introduction to Stimulated Emission Depletion Microscopy

In 1873, Abbe[1] linked the lateral (XY) resolution of a far-field optical microscope to the wavelength of light and defined the diffraction limit to $\sim\lambda/(2\mathrm{NA})$, where λ is the wavelength of the probing light, and NA is the numerical aperture of the light collection optics. For example, if visible light with a wavelength of 550 nm is used for imaging, then the smallest distance that can be resolved for a pair of point objects is ~200 nm using common wide-field optical microscopes.[2]

Almost a century later, the confocal concept was introduced by Minsky to improve optical slicing capability for specimens that are thicker than the focal plane.[3] In a typical confocal microscope, point illumination is used and a pinhole is placed before the detector to reject out-of-focus fluorescence background. Images are reconstructed pixel-by-pixel by raster scanning the sample (or the beam) with respect to the beam (or the sample). In the limiting case with an infinitely small pinhole, the lateral resolution can be improved by a factor of $\sim\sqrt{2}$. In practical cases where the pinholes need to be sufficiently large to let enough photons go through, the improvement in lateral resolution is very limited. However, the information content in the vertical direction is significantly increased compared to standard light microscopy because of the effective rejection of the out-of-focal plane fluorescence background and the ability to scan slices in the axial direction.

While there is no argument about the usefulness of epi-illumination or confocal microscopy, many cellular processes involve functional domains that have a characteristic length scale on the tens of nanometers or less. Clearly, these processes cannot be resolved using conventional epi- or confocal fluorescence microscopy. To break the diffraction limit in the far field, several types of "super-resolution" optical microscopies were developed.[4–6] The term super-resolution is popularly used to refer to optical resolution that is below the diffraction limit, which is ~200 nm laterally or ~500 nm axially.

Stimulated emission depletion (STED) microscopy is one type of far-field optical technique demonstrated to provide subdiffraction resolution. Generally, an excitation laser beam and a depletion laser beam are required in STED microscopy. The depletion laser beam is shaped to have a donut profile in the focal plane and overlapped with the excitation laser beam so that the STED process turns off the fluorophores at the outer rim of the excitation spot.[7] This depletion reduces the size of the focal plane fluorescence spot, improving the lateral resolution significantly. Figure 1(a) shows the ideal spatial intensity profiles of the excitation and depletion laser beams and the simulated collection spot in a STED microscope. The selection of the excitation and depletion laser wavelengths depends on the absorption and emission properties of the fluorophore used. Figure 1(b) shows an exemplary setup of a STED microscope with 488- and 592-nm laser lines for excitation and depletion, respectively. Both laser lines are expanded using sets of lenses (L) to slightly overfill the objective back aperture so that the full NA of the objective is utilized. The excitation laser beam is circularly polarized by a quarter-wave plate (QWP) to achieve the best excitation beam profile in the focal plane. To achieve the best donut-shaped depletion beam profile, a combination of a vortex plate, a Glan-type polarizer, and a QWP is applied in the depletion laser path. The fluorescence signals are selected by proper dichroic mirrors (DCLP and DCSP) and a bandpass filter. A notch filter is applied to greatly cut down the diffusive depletion laser scattering from the fluorescence signal. The fluorescence signal is then focused onto a confocal pinhole and collected by an avalanche photodiode detector that has a

*Address all correspondence to: Frances S. Ligler, E-mail: fsligler@ncsu.edu or Gufeng Wang, E-mail: gufeng_wang@ncsu.edu

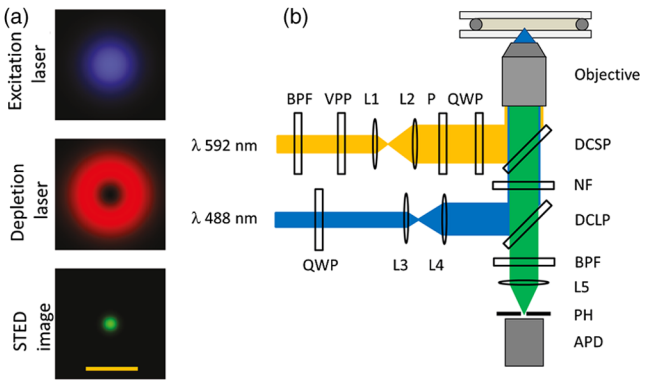

Fig. 1 Schematics of stimulated emission depletion (STED) microscopes. (a) Intensity profiles of the excitation, depletion, and collection spots. Scale bar: 500 nm. Reprinted figure with permission from the American Chemical Society.[8] (b) Schematic of a CW-STED microscope. Excitation is provided by a 488 nm laser line from an Ag^{+} laser and depletion by a 592-nm fiber laser. DCSP: dichroic mirror (short pass); VPP: vortex phase plate; BPF: bandpass filter; P: polarizer; L: lenses; QWP: quarter-wave plate; NF: notch filter; DCLP: dichroic mirror (long pass); PH: pinhole; APD: avalanche photodiode detector. Reprinted figure with permission from the American Institute of Physics.[9]

high quantum yield. Images are reconstructed by scanning the sample one pixel at a time. Two approaches are frequently used for scanning: sample scanning and beam scanning. Recently, scanning multiple pixels at a time is also reported for STED and relevant microscopic techniques, which will be discussed in Sec. 4.

In theory, the lateral spatial resolution of a STED microscope depends on the excitation and depletion laser wavelengths, the fluorescence lifetime of the dye, and the depletion laser power, with a theoretically unlimited resolution. The lateral resolution of a STED microscope δ with an ideal depletion beam is given by

$$\delta = \frac{\lambda}{2\mathrm{NA}} \frac{1}{\sqrt{1 + I_0/I_s}}, \tag{1}$$

where λ is the excitation wavelength, I_0 is the peak intensity of the depletion beam, and I_s (which depends on the intrinsic properties of the fluorophore such as fluorescence lifetime depletion cross section, etc.) is the characteristic intensity of the depletion laser beam at which the fluorescence emission is reduced to half of that in the absence of depletion. Equation (1) predicts that STED resolutions can be improved by increasing the I_0/I_s ratio, either by increasing the depletion laser power I_0 or by decreasing I_s, e.g., new fluorophores.[5] I_0 cannot be increased infinitely because photobleaching becomes significant at high power. I_s for commonly used fluorophores is in the range of 20 to 100 $\mathrm{MW/cm^2}$ and practical I_0 is in the range of 10 to 50 $\mathrm{GW/cm^2}$.[10]

In practice, the spatial resolution of a STED microscope is strongly dependent on the quality of the depletion beam profile, i.e., the darkness in the center kernel of the depletion beam and the intensity slope at the internal edge of the depletion donut. The effect of the intensity slope on the resolution can be accounted by introducing a factor "a" by the factor I_0/I_s in Eq. (1). A comprehensive study of origin of inverse square root dependence of spatial resolution on I_0/I_s and "a" factors was discussed by Harke et al.[11] The donut beam can be generated using several methods;[12–16] the most common approach nowadays is to use vortex phase plates that produce a phase ramp of 0 to 2π or 0 to π, respectively. Nonideal situations (e.g., mismatch between the laser wavelength and the phase plate, imperfect Gaussian beam, misalignment between the laser and the phase plate, polarization mismatch between the laser and the phase plate, and optical aberrations[17]) can contribute to the residual intensity in the center kernal,[9,18–20] and can negatively affect the predicted resolution. Neupane et al.[9] systematically characterized the impact of a nonideal depletion beam on the STED resolution; improving the spatial resolution requires a finely tuned donut beam. STED microscopy can be built in different modalities (please see Sec. 2). The best lateral resolution reported so far is ~6 nm when imaging nitrogen vacancy color centers in diamonds using a pulsed STED (p-STED) microscope.[21] Lateral resolutions in the range of 20 to 100 nm have been reported for biological samples.

Compared to other high resolution techniques, e.g., near-field scanning optical microscopy, atomic force microscopy (AFM), and electron microscopic techniques (TEM/SEM),[22,23] far-field super-resolution optical microscopies have the advantage of being nondestructive, potentially nonintrusive, and continuous for extended periods. In recent years, super-resolution has also been achieved using several other contemporary techniques, including structured illumination microscopy (SIM)[24,25] and its variant nonlinear saturated structured illumination microscopy (SSIM),[25,26] stochastic optical reconstruction microscopy - (STORM)[27,28] and photo-activated localization microscopy (PALM and 3D-PALM),[29] and other methods.[5,30–32] Each of these methods has its own strengths and limitations and can be appropriate for different applications.[4,6,23,33,34] STED microscopy is unique because it offers better spatial resolution than SIM and higher temporal resolution than STORM/PALM. Thus, it is especially useful to monitor dynamic biological processes in live cells or tissue when a resolution of several tens of nanometer is required. Some observations so far are only possible using STED techniques, and these applications are highlighted in the following discussion.

2 Different Modes of STED Microscopy and their Applications

Depending on the excitation and depletion schemes used, STED microscopes can have different designs. These designs accommodate the use of three different approaches for excitation: pulsed lasers, continuous wave (CW) sources, and two-photon (2P) illumination.

2.1 *STED Microscopy with Pulsed Laser Sources*

Since the theoretical demonstration of STED microscopy in 1994,[7] the first STED microscope with a subdiffraction-limited resolution was achieved in the pulsed mode in 1999.[35] To obtain super-resolution, precise time delays between the excitation and the depletion laser pulses are required in addition to the perfect overlap of two lasers at the focal plane. Since the first introduction, the strengths of such microscopes in resolving nanoscopic structures in live and fixed cells have been demonstrated by several research groups.[36–43]

The p-STED microscopy is widely used in studying fixed biological cells. A particularly interesting demonstration of p-STED microscopy resolved the organization of the protein subunits of mitofilin, MINOS1, and CHCHD3 residing in mitochondrial-inner-membrane-organization-system (MINOS)

in different chemically fixed cell types.[41] Jans et al.[41] labeled the subunits with antibodies and found that MINOS formed periodically organized nonfilamentous structures in mammalian cells but filaments in yeast cells. Sieber et al.[37] used p-STED microscopy to observe the formation of syntaxin clusters 1 and 4 in the plasma membrane of fixed cells. Syntaxins 1 and 4, respectively, are the sites where secretory vesicles and caveolae fuse. Contrary to the prevailing views that lipid phases are mandatory for cluster formation where cholesterol is responsible for cluster integrity in a plasma membrane, p-STED microscopy studies showed that the native lipid phases are not sufficient to provide correct cluster formation. The authors suggested that in addition to lipid phases, the syntaxin clustering involves protein–protein interaction with cytoplasmic SNARE protein motifs. Yang et al.[39] used p-STED microscopy to probe the arrangement of adenyl cyclase type III (ACIII; a protein that helps in signaling) and intraflagellar transport-88 (IFT88; a core protein required for cilia formation) proteins in cilia of chemically fixed human fibroblast cells. Immunostaining with Alexa Fluro488-conjugated antibodies revealed that ACIII forms periodic patterns along the cilia but IFT88 forms Y- or triangle arrangements.

The localization, composition, and turnover of several proteins at synaptic and pre-/post-synaptic sites play a significant role in the proper functioning of the brain.[44] Recent studies with fixed cells and p-STED microscopy imaged such proteins in different types of cells.[38,45–48] Willig et al.[49] used p-STED microscopy to study the fate of ATTO 532-antibody labeled synaptotagmin I—a protein residing in the synaptic vesicle membrane—after synaptic vesicles are exocytosed. The observation of similarly sized patches of synaptotagmin in both surface-exposed and internalized vesicle pools suggested that synaptotagmin, instead of diffusing away, remains clustered in the plasma membrane after vesicle exocytosis. Blom et al.[45] studied the distribution of $\alpha 3$ isoform of Na^+/K^+-ATPase—a protein responsible for actively transporting Na^+ and K^+ ions across the plasma membrane—in goat-anti-mouse Alexa-594 labeled dendritic spines of striatal neural cells. They found that the $\alpha 3$ isoform is discontinuously distributed in the spine heads and necks and within the connecting dendritic structures. They suggested that such a distribution of the protein may be responsible for generating local Na^+/K^+ gradient and could assist in functional interaction with other synaptic proteins. Kellner et al.[47] used p-STED microscopy to reveal the supermolecular aggregates of acetylcholine receptor (AChR) residing on the membrane surface of Chinese hamster ovary (CHO)-K1/A5 cells. The AChR receptor is found in neuromuscular junctions and believed to play a critical role in fast synaptic transmission. The AChR was labeled either with Alexa 594-α-bungarotoxin (αBTX) or anti-AChR plus ATTO 532-secondary antibody. Cholesterol-rich membrane domains are believed to be critical in proper organization and functionality of AChR receptor. They found that in cholesterol-depleted cells, the AChR complex was larger than in cells with normal cholesterol. Based on this data, the authors suggested that cholesterol plays an important role in organization of a AChR receptor.

STED microscopy has the potential to study various intracellular processes in real time and in "living" cells. Live-cell STED imaging can be achieved by fusing green fluorescent proteins (GFPs) to target proteins or using self-labeling proteins that covalently bind to organic dyes. Lateral resolutions in the range of 40 to 100 nm within live mammalian cells were reported. For example, using a novel hAGT tagging protein that covalently binds to various fluorophores, Hein et al.[50] resolved fine tubular protein structures located in cytoskeleton (vimentin and microtubule-associated protein) and in cell membrane (caveolin and connexin-43) of live Potoroo kidney (PtK2) cells. In the work of Nagerl et al.,[51] p-STED microscopy was used to study chemically induced morphological change of dendritic structures in live hippocampal neural cells. Tiny morphological changes in spine head and neck of the neurons were observed at a frame rate of ~20 s/frame (field of view: 10×10 μm) using genetically labeled yellow fluorescent protein (YFP) as the STED probe. The authors suggested that such morphological changes reflect the plasticity of synaptic connections. Using a glycerol immersion objective, Urban et al.[52] demonstrated that dynamic actin structures in dendrites and spines in live hippocampal neuron slices can be monitored at various depths from the tissue surface. The actin was genetically labeled with Lifeact-EYFP. Figure 2(a) shows p-STED images collected at various depths. Actin dynamics were recorded at a frame rate of 11 s/frame (field of view: 20×20 μm) in spine, neck, and head structures. It was shown that in contrast to the controls, chemical long-term potentiation induces a large number of spine necks to widen in neuron cells. The observation of the change in morphology of the actin-based structures showed that it is possible to monitor neuronal activity deep inside brain tissue. Hein et al.[53] used p-STED microscopy to visualize the structural changes in the endoplasmic tubules of live mammalian PtK2 cells genetically labeled with YFP citrine. By recording the consecutive images at a frame rate of 10 s/frame (field view: 10×2.5 μm), formation and breaking enclosures in tubules were observed in the endoplasmic reticulum of live cells [Fig. 2(b)]. Westphal et al.[46] studied the diffusion of fluorescently labeled synaptic vesicles inside the axons of live hippocampal neurons. Using a small field of view (2.5×1.8 μm), a frame rate of 25 frames/s was achieved, which provided the temporal resolution for mapping the vesicle movement in both bouton and nonbouton areas. It was found that vesicle movement is substantially faster in the nonbouton areas.

The above studies show that STED microscopy provides an effective way to monitor highly dynamic biological processes in "live" cells or tissue at a spatial resolution of several tens of nanometers and a temporal resolution of a few to a few tens of frames per second (fps). Notably, most of the above observations in live cells so far can only be made using STED techniques. For example, the STED microscopy made it possible to observe the fast movement of crowded synaptic vesicles in live hippocampal neurons, which is critical to understand how neurons work under physiological conditions.[46] The observation of subtle morphological change of actin-based structures upon chemical long-term potentiation opens the door to investigate actin dynamics and neuronal activity deep inside brain tissue.[52]

2.2 *STED Microscopy with CW Laser Sources*

A simplified version of STED microscopy uses CW laser sources for both excitation and depletion. Since there is no need for synchronizing the lasers, the setup is technologically simpler to implement. It has been demonstrated in theory and in experiments that CW-STED microscopy offers resolution similar to p-STED microscopy.[9,54] The first experimental realization of CW-STED microscopy was demonstrated by using green/red (532/760 nm) excitation/depletion laser pairs.[55] By imaging nitrogen vacancies in diamonds, lateral resolution of

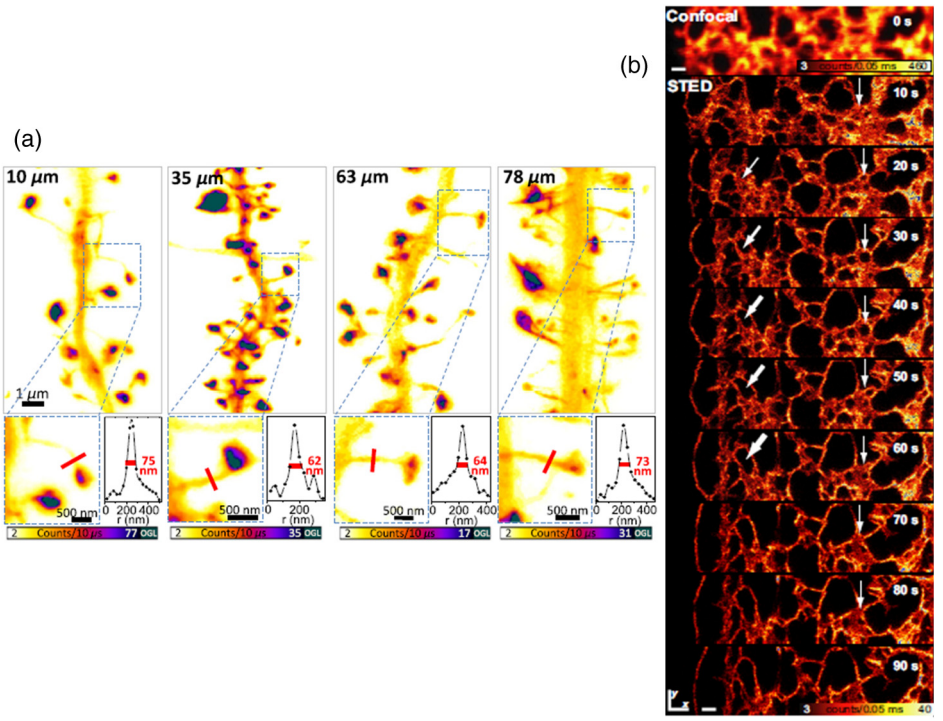

Fig. 2 Live cell STED imaging. (a) p-STED resolves the distribution of actin in dendrites and spines in hippocampal neuron slices at various depths. For imaging, actin was labeled genetically with yellow fluorescent protein (YFP). STED images recorded at depths of 10, 35, 63, and 78 μm are shown in the large frames (left to right). The insets show the zoom of one of the narrowest structures along with line profiles, demonstrating the resolution at various depths. All the numbers in the insets are in nanometers. Reprinted figure with permission from the Biophysical Society.[52] (b) Dynamics of the endoplasmic reticulum tubules in live mammalian PtK2 cells imaged with p-STED microscopy at time intervals of 10 s. Confocal image at time 0 is shown in the topmost slice. For imaging, the tubules were genetically labeled with YFP citrine. The arrows in each slice show the most prominent structural changes during the time-lapse study. Scale bar: 500 nm. Reprinted figure with permission from the National Academy of Sciences.[53]

~30 nm was reported. Later, a STED microscope that uses blue/orange (488/592 nm) fiber laser pairs as excitation/depletion was demonstrated.[56] Resolution of ~60 nm was achieved in imaging Alexa 488- and fluorescein isothiocyanate-antibody labeled vimentin filaments in fixed PtK2 cells. The potential of this setup for live cell imaging was demonstrated by imaging endoplasmic reticulum of live PtK2 cells genetically labeled with fluorescent protein Citrine. Lateral resolution of 65 nm was reported. Since then, CW-STED setup has also been demonstrated by a few other groups.[9,57,58]

2.3 *STED Microscopy with Two-Photon Excitation*

Multiphoton excitation microscopy is a technique that provides high-depth imaging of tissue samples. In two-photon excitation microscopy, a fluorophore is excited with a femtosecond laser pulse having a wavelength twice that for single-photon (1P) excitation. As compared to 1P excitation, 2P-excited fluorescence is intrinsically more localized in the axial direction. In imaging thick samples, the out-of-focal-plane signal is significantly suppressed, providing better optical sectioning capability. The 2P excitation microscopy is a mature technology, and its utility has been demonstrated for imaging from thin samples (e.g., plated cells) to millimeter-thick samples (e.g., brain slices). The detailed description of 2P excitation microscopy and its applications have been covered elsewhere.[2,59–61]

The combined use of 2P excitation with STED microscopy provides a new opportunity for imaging thick samples with sub-diffraction-limited resolution. The 2P-STED microscopes can be constructed using either a 2P-CW-STED or a pulsed laser 2P-p-STED as a depletion source. The first 2P-CW-STED microscope was demonstrated by Moneron and Hell[62] in imaging the distribution of antibody-ATTO565-labeled NFκB receptor, an important transcription regulator, in nucleus of fixed PtK2 cells. Later, the suitability of such a setup for deep tissue imaging was demonstrated by imaging the morphology of Alexa-Fluor-594 labeled dendritic spines in fixed hippocampal brain tissue located up to 100 μm below the slice surface.[63]

The 2P-p-STED microscopy was first demonstrated by resolving GFP-tagged caveolar vesicles in a chemically fixed CHO cell.[64] A simplified version of 2P-p-STED that uses a single laser line for both 2P excitation and 1P depletion was also demonstrated recently for 4-(dicyanomethylene)-2-methyl-6-(p-dimethylaminostyryl)-4H-pyran (DCM) dyes.[65] The possibility of using this setup in cellular imaging was demonstrated by imaging the antibody-ATTO 647N-labeled microtubules in fixed PtK2 cells.[66]

3 Improving Axial Resolution of STED Microscopy

Improving the axial resolution of confocal-type STED microscopy remains a challenge. With all parameters optimized, the

commonly used $0 < \varphi < 2\pi$ vortex phase plates offer excellent lateral resolution in the range of 20 to 50 nm. There is no resolution improvement in the axial direction because the phase plate generates a hollow, tube-like point spread function (PSF) with zero depletion laser intensity along the optical axis. More clearly, depletion and hence resolution improvement is only possible along the lateral direction. In an alternative approach where $0 < \varphi < \pi$ vortex phase plates are used, the STED laser gives a three–dimensional (3-D), hollow spheroid-like PSF, which improves the axial resolution by a factor of 6 (~150 nm) as compared to confocal fluorescence microscopy in imaging vacuolar membranes of live yeast cells labeled with RH-41.[67] However, the lateral resolution improvement is very limited (~120 nm, a factor of 2) because the STED beam PSF has a relatively wide and flat intensity profile in the center at the focal plane. Similar resolution improvement was also reported in imaging endoplasmic reticulum tubules of live mammalian PtK2 cells genetically labeled with YFP citrine.[53] More recently, a $0 < \varphi < 2\pi$ and $0 < \varphi < \pi$ phase plates were used together to achieve the best axial and lateral resolutions simultaneously. Axial and lateral resolutions of 100 and 45 nm, respectively, were reported in imaging immunostained microtubules in PtK2 cells.[9]

Two multimodal approaches have been recently realized to achieve better axial resolution in STED microscopy. In the first approach, total internal reflection fluorescence (TIRF) imaging mode is coupled to STED microscopy.[68] TIRF utilizes the evanescent field as the excitation, which has a penetration depth of ~100 nm. The success of this multimode imaging technique was demonstrated by imaging antibody ATTO 647N-labeled microtubules in fixed PtK2 cells[68] and by studying the diffusion of fluorescent lipid analogs in synthetic lipid bilayers.[69] Both axial and lateral resolutions down to ~50 nm were demonstrated.[69] In addition, STED-TIRF also has less photobleaching to the sample than standard STED. However, STED-TIRF can only image features adjacent to the waveguide surface. We anticipate that STED-TIRF microscopy can be an important technique for studying the structures as well as dynamic diffusion of nanometer sized objects on or near the surface of a living cell.

Another approach to achieve better Z-resolution in STED microscopy is to couple it with 4Pi microscopy. In a 4Pi microscope, the same focal plane of a sample is illuminated and/or collected using two opposing objective lens, i.e., one above and one below the sample. Each objective lens can have a maximum theoretical collection solid angle of 2Pi, thus a total collection angle of 4Pi. The image is reconstructed by the superposition of signals collected from both optical paths. Using this approach, an axial resolution of ~80 nm was demonstrated by imaging a mitochondrial network in live yeast. The mitochondrial matrix protein was labeled with GFP.[70] In another study, by coupling p-STED to 4Pi microscopy, both axial and lateral resolutions of ~50 nm were reported.[71] This setup has been successfully used in imaging the 3-D distribution of antibodies labeled with NK51 (an orange-emitting dye) bound to TOM20 protein—an import receptor protein involved in the initial recognition of preproteins—in the mitochondria of fixed mammalian Vero cells. By imaging multiple XY images at various depths ($Z = -240$ to $+240$ nm), a 3-D image of TOM20 clusters was reconstructed, which revealed that protein clusters are localized at the rim of the organelle. The STED-4Pi microscope is very promising in the study of biological samples as it offers isotropic XYZ resolutions. However, this technology is limited to thin samples only a few micrometers thick.

4 Improving Temporal Resolution of STED Microscopy

Imaging speed, usually measured in fps, is a critical factor in studying highly dynamic biological processes. The imaging speed of a STED microscope in principle is identical to that of a confocal laser scanning or stage scanning fluorescence microscope. In both methods, images are collected pixel by pixel and the full-field images are then reconstructed. In practice, imaging speed depends on several parameters including signal-to-noise ratio, size of the field-of-view, and maximum scanner speed.[2] Video rate imaging (28 fps) of vesicle movement in a $\sim 2 \times 2$ μm^2 field of view was realized by bidirectional scanning: the excitation and depletion beam scanning in one direction using a 16-kHz resonant mirror, and sampling scanning in the perpendicular direction using a piezo actuator.[46] A mathematical filter was used to improve the confidence of vesicle recognition.

The pixel-by-pixel imaging approach is the rate-limiting step in STED imaging. To improve the imaging speed of STED microscopy, a parallel approach was demonstrated.[72] This approach splits the original excitation/depletion laser beams into four excitation/depletion pairs to scan the sample and uses four point detectors to collect the signals simultaneously. By imaging KK114-labelled tubulin strands in a fixed mammalian PtK2 cell, this approach demonstrated four times faster scanning speed without significantly compromising the resolution. This approach is in theory promising because potentially it can be extended to collect multiple spots on the sample simultaneously. However, super-resolution imaging based on STED requires high-depletion laser power. With current commercially available lasers, it is impractical to further split the depletion beam while keeping the desired resolution.

A recent variation of STED microscopy breaks this barrier imposed on depletion laser power. As discussed in Sec. 1, STED-type super-resolution is achieved by converting the excited fluorophores to an "off" state by the STED process. Alternatively, the off-switching can be achieved through other mechanisms but at significantly low power. One such mechanism is reversible photo-switching, in which a moiety of the fluorophore rearranges, e.g., cis- to trans-flipping, in the presence of light at specific wavelength(s), and the fluorophore converts to a dark state. The imaging technique using the photo-switching to improve resolution is named reversible saturable optical fluorescence transitions (RESOLFT) microscopy. The photo-switching process is usually slow as compared to the STED process.[5] However, it requires a laser power thousands of times weaker, allowing the off-switching laser to be split into many copies. Recently, parallel RESOLFT imaging that uses as many as 100,000 focal plane donuts for scanning was reported.[73] Imaging speed of ~2 fps was achieved on a 50×50 μm^2 area with a lateral resolution of 80 nm in imaging keratin filaments genetically labeled with a switchable variant of enhanced green fluorescent protein (EGFP) protein in live PtK2 cells. The temporal resolution is reported to be limited by camera readout time and the switching time of fluorophores.[73]

5 Multicolor STED Microscopy (m-STED)

Multicolor microscopy allows the study of multiple cellular structures or events at the same time. It is proven to be very useful in the study of correlation between multiple cellular moieties and the degree of interactions in live cells in the 3-D space.[74–76] Compared to single-color microscopy, multicolor

imaging requires labeling using multiple fluorophores with distinct spectral properties and excitation/collection at different color channels. In recent years, different types of multicolor super-resolution microscopy have been demonstrated in fixed and live cells; examples include multicolor-SIM,[77] multicolor-STORM,[78,79] and multicolor-STED (m-STED).[80–85]

The first type of m-STED, which requires different excitation/depletion laser pairs for each fluorophore, was demonstrated by simultaneously resolving ATTO-647N-labeled synaptophysin (red) and ATTO-532-labeled syntaxin 1 (green) synaptic protein nanostructures in fixed neural cells.[80] The distribution of two differently labeled proteins was revealed simultaneously with a resolution of 25 to 35 nm in the focal plane. This setup can be extended to three channels: first two channels were separated on the basis of fluorescent lifetimes of dyes with similar absorption and emission spectra, and the third channel is separated on the basis of color. This setup was successfully used in colocalization lamin immunostained with KK114, tubulin immunostained with ATTO-647N, and clathrin immunostained with ATTO 590 in fixed mammalian PtK2 cells [Fig. 3(a)].[85]

The above design requires two laser lines for each color channel, which is difficult to implement practically. The recent trend of m-STED imaging is to reduce the number of laser lines by carefully selecting dyes.[81–84] For example, Pellett et al.[82] labeled epidermal growth factor (EGF) and EGF receptor (EGFR) on live human embryonic kidney (HEK 293) cell membrane with two different dyes using SNAP and CLIP tags, where

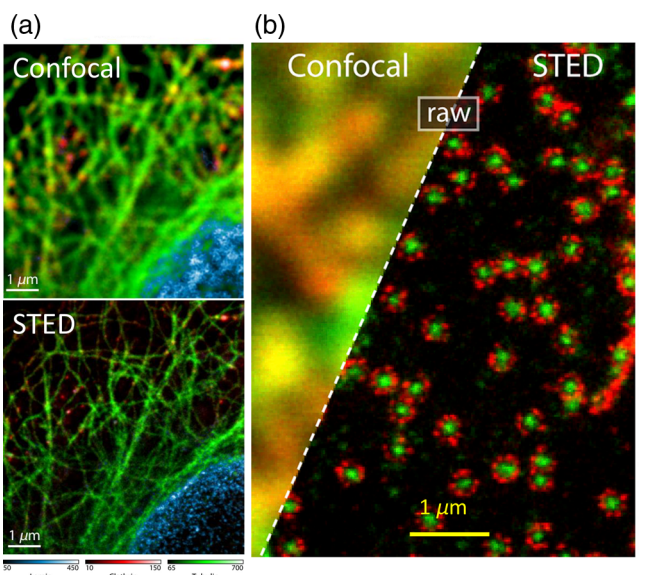

Fig. 3 Multicolor STED imaging. (a) STED microscopy in three colors to localize the distribution of lamin, tubulin, and clathrin in fixed PtK2 cells. The lamin and tubulin were labeled with antibody conjugated to KK114 and ATTO 647N dyes, respectively. The dyes were differentiated on the basis of their fluorescent lifetimes. The clathrin was labeled with ATTO 590. ATTO 590 has a different spectrum from the rest of the dyes and was selected spectrally. Reprinted figure with permission from The Optical Society.[85] (b) Dual channel (yellow and red) STED microscopy reveals octametic arrangement of peripheral transmembrane GP210 protein around core protein in a nuclear pore complex in immunolabeled Xenopus cells. The central and peripheral proteins were, respectively, labeled with antibody-ATTO 594 and antibody-KK114, and detected in two channels (620 ± 20 and 670 ± 20 nm). Two different laser lines were used for excitation, but the depletion was achieved with the same laser line. Scale bar: 1 μm. Reprinted figure with permission from the Biophysical Society.[81]

SNAP- and CLIP-tags are proteins fused to target protein of interest and further covalently tagged with a suitable ligand, such as a fluorescent dye. The two dyes (e.g., EGFR-SNAPf-Chromeo494 and EGF-CLIPf-ATTO 647N) can be excited at 532 and 640 nm, respectively, and depleted at the same wavelength by a Ti:sapphire laser. Resolutions of 78 nm and 82 nm for the two-color STED system were reported.[82] Using a similar setup with 595-nm and 640-nm excitation, respectively, and 775-nm depletion, Gottfert et al.[81] imaged the nanoscopic details of nuclear pore complexes (NPCs) in fixed immunolabeled Xenopus cells at a resolution of 20 nm [Fig. 3(b)]. The individual NPC was successfully resolved, which was shown to have an eightfold symmetry of antibody ATTO594-labeled GP210 proteins arranged around antibody-KK114 labeled central core protein in a nuclear pore. The resolution of 20 nm is so far the best reported STED resolution in cell studies.

The m-STED microscopy can be further simplified to contain one excitation and one depletion lasers. Tonnesen et al.[83] carefully selected GFP pairs, e.g., YFP and enhanced GFP, so that they can be excited and depleted with the same laser pair but their fluorescence collected in separate color channels. Examples of sequential STED imaging axonal boutons and dendritic spines in living organotypic brain slices were given. The reported resolutions are 86 nm with YFP and 77 nm with EGFP labels.

In an alternative approach, Willig et al.[84] developed a pair of reversibly photo-switchable fluorescent variants of Padron and Dronpa proteins. These two proteins have similar emission spectra but opposite switching behavior when exposed to 405 nm light. Thus, the two dyes can be collected alternatively using the same 488-nm excitation/595-nm depletion lasers. The success of this approach was demonstrated by imaging the distribution of Map2 (a microtubule cytoskeleton protein) and connexin37 (a key component of gap junctions) proteins in live PtK2 cells. The full width at half-maximum resolutions were ~70 nm and ~90 nm for Padron- or Dronpa-labeled structures, respectively. The lower resolution observed for Dronpa-labeled structures is possibly due to the shorter fluorescence lifetime of Dronpa (0.8 ns versus 3 ns for Padron) and that the fluorescence spectrum of Dronpa is ~4 nm blue-shifted that decreases the depletion cross section.

6 Practical Aspects of STED Microscopy

Compared to other high-resolution microscopies, the strength of STED microscopy is that it can resolve nanostructures in live cells in real time and *in situ*. To take advantage of this property fully, several research groups are actively working on practical issues of STED microscopy.

6.1 *Phototoxicity*

The high-depletion laser power up to several tens of GW/cm^2 used in STED microscopy can pose problems of phototoxicity to live biological samples. Photobleaching of dyes also limits prolonged imaging. The goal is to decrease the depletion laser power without sacrificing the spatial resolution. For example, Vicidomini et al.[86] demonstrated that by using pulsed excitation, CW depletion, and time-gated detection in STED microscopy, the depletion laser power can be decreased by a factor of 3 without compromising the resolution. In another effort, Hao et al. proposed in theory that an alternate image inverting interferometry method can be used to achieve a smaller donut crest than those obtained from commonly practiced vortex phase plates. It

is predicted that this method can decrease the depletion laser power by 33%.[87]

RESOLFT seems to be an effective technique to lower the off-switching laser power and subsequent photodamage to the biological sample and the dyes. The characteristic laser intensity I_s for photo-switchable probes is thousands of times smaller than those of STED-based probes. It means that the off-switching laser power can be lowered by thousands of times, a level similar to the excitation laser power, while keeping comparable resolution. Although the photo-switching process is relatively slow, recent parallel RESOLFT imaging demonstrates excellent speed in studying nanoscopic processes in live cells while imposing minimal phototoxicity.[73]

Finding a STED probe that is less prone to photobleaching and/or can be depleted with minimal laser power is of equal importance to decreasing the laser power. Despite the current existence of STED dyes acceptable for use with fixed cells,[88] continual efforts are made toward discovering new probes for use in STED microscopy.[42,89] The feasibility of using CdSe/CdS quantum dots as a photostable label has also been recently explored;[90] lateral resolution of ~40 nm was reported on air–glass interface but cell studies and cytotoxicity were not evaluated.

Recently, new families of STED dyes that are least toxic to live cells and bind very specifically to cytoskeleton proteins are also reported.[91] Periodic ring-like structures of actins in neuron axons were observed. An ideal STED probe should pose minimum cytotoxicity, can be depleted with minimal depletion laser power, and is sufficiently photostable that imaging over prolonged time is possible.

6.2 *Selection and Utilization of Lasers*

Another factor to consider is the cost of STED microscopes. One major component in the total cost of a STED microscope is the laser system. The first pulsed STED microscope was constructed using a mode-locked Ti:sapphire laser as the depletion source and its second harmonic signal as the excitation.[35] Later, STED microscopes were constructed using mode-locked Ti:sapphire laser/Ti-sapphire pumped optical parametric oscillators[67] or paired pulsed laser diodes as the excitation and depletion sources.[92] These microscopes need two pulsed lasers or laser components, which greatly adds to the cost and technological complexity of the STED microscope. The use of CW excitation reduces the cost compared to the integration of pulsed lasers. However, for each color channel, two laser lines including a high-power depletion laser source with an excellent beam profile are still needed. Current laser output is either nontunable or has very narrow tunable range. Thus, there is a significant additional cost as the number of color channels in the STED microscope increases.

To make the most use of the expensive laser components, alternative laser sources that provide tunable output will be promising. A STED setup that uses a tunable super-continuum light source has been demonstrated and made commercially available.[93] In this setup, a part of the output from a mode-locked Ti:sapphire laser is sent through a polarization-maintaining microstructured optical fiber to generate the broad super-continuum that serves as the tunable excitation after optical filtering. The rest of the output from the Ti:sapphire laser is temporally stretched and used as a depletion source. STED with super-continuum light source provides low cost and compact solution for STED microscopy. Such a setup has been used by other groups in STED fluorescence lifetime imaging.[36,43]

Another approach that uses discrete multicolor-stimulated Raman scattering light as the depletion source has been applied in STED microscopy.[94] The output of a Q-switched microchip laser at 532 nm is sent through a polarization-maintaining single-mode fiber, which emits seven discrete laser lines in the range of 532 to 620 nm. It was demonstrated experimentally that all these laser lines can work as depletion sources for different dyes in the presence of a common excitation source from a blue (477 nm) laser diode.

7 Concluding Remarks and Future Perspectives

STED microscopy can image biological samples with a resolution of a few tens of nanometers. With careful and creative design, resolution improvement can be achieved in all three dimensions. The biggest advantage of STED microscopy is that it can be applied in live cells in real time and *in situ*.

There are still significant issues to be addressed prior to widespread use of STED microscopy. Recently, the improvements in STED microscopes have reduced the lateral and axial resolutions, provided for temporal resolution, and facilitated imaging deeper into tissues. The future development of STED microscopy, from our perspective, will require the following hurdles to be addressed: (1) find new dyes that are more resistant to photobleaching and that can be depleted at low-light intensity levels. Such dyes will provide the means to observe biological samples on a long-term basis. (2) Improve the accessibility of STED microscopes to common research labs. Reducing the cost of STED microscopes is the goal, which will be assisted by the development of appropriate laser technologies. (3) Improve the usability of STED microscopes. Mechanical drifting of optical elements causes misalignment of both laser beams, thus the loss of super-resolution. Retuning the STED microscope usually requires well-trained personnel devoting time on a frequent basis. Creative design and improved optical engineering are required to overcome this important practical issue. (4) Combine STED microscopy with other techniques to obtain the complementary information on the samples. In recent years, correlative and multimodal approaches that combined STED microscopy with other probing techniques have been demonstrated. For example, STED microscopy has been coupled to AFM (so named STED-AFM) to image ATTO-647-immunolabeled microtubules in fixed HeLa and kidney cos7 cells.[95,96] STED-AFM offers high-resolution fluorescent images with molecular specificity, topological images of the sample, and information about the mechanical properties, such as elasticity and local stiffness of microtubule filaments, in the same sample space.[95,96] In another approach, STED microscopy has been coupled with optical tweezers to integrate both nanoscale resolution and precise mechanical control of the sample.[97] This setup successfully revealed the diffusion dynamics of ATTO 647N-labeled protein on optically stretched DNA *in vitro*. We believe that such complementary approaches can provide valuable information about biological samples that has not been previously measureable.

Acknowledgments

Funding for this collaboration was provided by a North Carolina State University Research and Innovation Seed Funding grant (G. W., PI).

References

1. E. Abbe, "Beitrage zur Theorie des Mikroskops und der mikroskopischen Wahrnehmung," *Arch. Mikroskop. Anat.* **9**, 413–468 (1873).
2. A. S. Stender et al., "Single cell optical imaging and spectroscopy," *Chem. Rev.* **113**(4), 2469–2527 (2013).
3. M. Minsky, "Memoir on inventing the confocal scanning microscope," *Scanning* **10**(4), 128–138 (1988).
4. B. Huang, H. Babcock, and X. Zhuang, "Breaking the diffraction barrier: super-resolution imaging of cells," *Cell* **143**(7), 1047–1058 (2010).
5. S. W. Hell, "Far-field optical nanoscopy," *Science* **316**(5828), 1153–1158 (2007).
6. D. Toomre and J. Bewersdorf, "A new wave of cellular imaging," in *Annual Review of Cell and Developmental Biology*, Vol. 26, R. Schekman, L. Goldstein, and R. Lehmann, Eds., pp. 285–314, Annual Reviews Palo Alto (2010).
7. S. W. Hell and J. Wichmann, "Breaking the diffraction resolution limit by stimulated emission: stimulated-emission-depletion fluorescence microscopy," *Opt. Lett.* **19**(11), 780–782 (1994).
8. M. A. Lauterbach et al., "Dynamic imaging of colloidal-crystal nanostructures at 200 frames per second," *Langmuir* **26**(18), 14400–14404 (2010).
9. B. Neupane et al., "Tuning donut profile for spatial resolution in stimulated emission depletion microscopy," *Rev. Sci. Instrum.* **84**(4), 043701 (2013).
10. D. Wildanger et al., "A compact STED microscope providing 3D nanoscale resolution," *J. Microsc.* **236**(1), 35–43 (2009).
11. B. Harke et al., "Resolution scaling in STED microscopy," *Opt. Express* **16**(6), 4154–4162 (2008).
12. M. Sakai et al., "Formation of a doughnut laser beam for super-resolving microscopy using a phase spatial light modulator," *Opt. Eng.* **43**(5), 1136–1143 (2004).
13. V. V. Kotlyar et al., "Generation of phase singularity through diffracting a plane or Gaussian beam by a spiral phase plate," *J. Opt. Soc. Am. A* **22**(5), 849–861 (2005).
14. P. Torok and P.R.T. Munro, "The use of Gauss-Laguerre vector beams in STED microscopy," *Opt. Express* **12**(15), 3605–3617 (2004).
15. N. Bokor and N. Davidson, "A three dimensional dark focal spot uniformly surrounded by light," *Opt. Commun.* **279**(2), 229–234 (2007).
16. N. Davidson and N. Bokor, "High-numerical-aperture focusing of radially polarized doughnut beams with a parabolic mirror and a flat diffractive lens," *Opt. Lett.* **29**(12), 1318–1320 (2004).
17. S. H. Deng et al., "Effects of primary aberrations on the fluorescence depletion patterns of STED microscopy," *Opt. Express* **18**(2), 1657–1666 (2010).
18. N. Bokor et al., "On polarization effects in fluorescence depletion microscopy," *Opt. Commun.* **272**(1), 263–268 (2007).
19. X. A. Hao et al., "Effects of polarization on the de-excitation dark focal spot in STED microscopy," *J. Opt.* **12**(11), 115707 (2010).
20. T. A. Klar, E. Engel, and S. W. Hell, "Breaking Abbe's diffraction resolution limit in fluorescence microscopy with stimulated emission depletion beams of various shapes," *Phys. Rev. E* **64**(6), 066611 (2001).
21. E. Rittweger et al., "STED microscopy reveals crystal colour centres with nanometric resolution," *Nat. Photonics* **3**(3), 144–147 (2009).
22. E. Betzig and J. K. Trautman, "Near-field optics: microscopy, spectroscopy, and surface modification beyond the diffraction limit," *Science* **257**(5067), 189–195 (1992).
23. L. Schermelleh, R. Heintzmann, and H. Leonhardt, "A guide to super-resolution fluorescence microscopy," *J. Cell Biol.* **190**(2), 165–175 (2010).
24. M.G.L. Gustafsson, "Surpassing the lateral resolution limit by a factor of two using structured illumination microscopy," *J. Microsc.* **198**(2), 82–87 (2000).
25. M.G.L. Gustafsson, "Nonlinear structured-illumination microscopy: wide-field fluorescence imaging with theoretically unlimited resolution," *Proc. Natl. Acad. Sci. U. S. A.* **102**(37), 13081–13086 (2005).
26. R. Heintzmann, "Saturated patterned excitation microscopy with two-dimensional excitation patterns," *Micron* **34**(6–7), 283–291 (2003).
27. B. Huang et al., "Three-dimensional super-resolution imaging by stochastic optical reconstruction microscopy," *Science* **319**(5864), 810–813 (2008).
28. M. J. Rust, M. Bates, and X. Zhuang, "Sub-diffraction-limit imaging by stochastic optical reconstruction microscopy (STORM)," *Nat. Methods* **3**(10), 793–796 (2006).
29. E. Betzig et al., "Imaging intracellular fluorescent proteins at nanometer resolution," *Science* **313**(5793), 1642–1645 (2006).
30. M. Hofmann et al., "Breaking the diffraction barrier in fluorescence microscopy at low light intensities by using reversibly photoswitchable proteins," *Proc. Natl. Acad. Sci. U. S. A.* **102**(49), 17565–17569 (2005).
31. M. G. Gustafsson, D. A. Agard, and J. W. Sedat, "I5M: 3D widefield light microscopy with better than 100 nm axial resolution," *J. Microsc.* **195**(1), 10–16 (1999).
32. H. Zhang, M. Zhao, and L. Peng, "Nonlinear structured illumination microscopy by surface plasmon enhanced stimulated emission depletion," *Opt. Express* **19**(24), 24783–24794 (2011).
33. P. Sengupta, S. B. van Engelenburg, and J. Lippincott-Schwartz, "Superresolution imaging of biological systems using photoactivated localization microscopy," *Chem. Rev.* **114**(6), 3189–3202 (2014).
34. B. O. Leung and K. C. Chou, "Review of super-resolution fluorescence microscopy for biology," *Appl. Spectrosc.* **65**(9), 967–980 (2011).
35. T. A. Klar and S. W. Hell, "Subdiffraction resolution in far-field fluorescence microscopy," *Opt. Lett.* **24**(14), 954–956 (1999).
36. E. Auksorius et al., "Stimulated emission depletion microscopy with a supercontinuum source and fluorescence lifetime imaging," *Opt. Lett.* **33**(2), 113–115 (2008).
37. J. J. Sieber et al., "The SNARE motif is essential for the formation of syntaxin clusters in the plasma membrane," *Biophys. J.* **90**(8), 2843–2851 (2006).
38. R. J. Kittel et al., "Bruchpilot promotes active zone assembly, Ca2+ channel clustering, and vesicle release," *Science* **312**(5776), 1051–1054 (2006).
39. T. T. Yang et al., "Superresolution STED microscopy reveals differential localization in primary cilia," *Cytoskeleton* **70**(1), 54–65 (2013).
40. L. Shuai et al., "Enhancing the performance of fluorescence emission difference microscopy using beam modulation," *J. Opt.* **15**(12), 125708 (2013).
41. D. C. Jans et al., "STED super-resolution microscopy reveals an array of MINOS clusters along human mitochondria," *Proc. Natl. Acad. Sci. U. S. A.* **110**(22), 8936–8941 (2013).
42. Y. Sivan et al., "Nanoparticle-assisted stimulated-emission-depletion nanoscopy," *ACS Nano* **6**(6), 5291–5296 (2012).
43. M. D. Lesoine et al., "Supercontinuum stimulated emission depletion fluorescence lifetime imaging," *J. Phys. Chem. B* **116**(27), 7821–7826 (2012).
44. D. Choquet and A. Triller, "The role of receptor diffusion in the organization of the postsynaptic membrane," *Nat. Rev. Neurosci.* **4**(4), 251–265 (2003).
45. H. Blom et al., "Spatial distribution of Na+-K+-ATPase in dendritic spines dissected by nanoscale superresolution STED microscopy," *BMC Neurosci.* **12**(16), 1471–2202 (2011).
46. V. Westphal et al., "Video-rate far-field optical nanoscopy dissects synaptic vesicle movement," *Science* **320**(5873), 246–249 (2008).
47. R. R. Kellner et al., "Nanoscale organization of nicotinic acetylcholine receptors revealed by stimulated emission depletion microscopy," *Neuroscience* **144**(1), 135–143 (2007).
48. M. Maglione and S. J. Sigrist, "Seeing the forest tree by tree: super-resolution light microscopy meets the neurosciences," *Nat. Neurosci.* **16**(7), 790–797 (2013).
49. K. I. Willig et al., "STED microscopy reveals that synaptotagmin remains clustered after synaptic vesicle exocytosis," *Nature* **440**(7086), 935–939 (2006).
50. B. Hein et al., "Stimulated emission depletion nanoscopy of living cells using SNAP-tag fusion proteins," *Biophys. J.* **98**(1), 158–163 (2010).
51. U. V. Nagerl et al., "Live-cell imaging of dendritic spines by STED microscopy," *Proc. Nat. Acad. Sci. U. S. A.* **105**(48), 18982–18987 (2008).
52. N. T. Urban et al., "STED nanoscopy of actin dynamics in synapses deep inside living brain slices," *Biophys. J.* **101**(5), 1277–1284 (2011).
53. B. Hein, K. I. Willig, and S. W. Hell, "Stimulated emission depletion (STED) nanoscopy of a fluorescent protein-labeled organelle inside a living cell," *Proc. Natl. Acad. Sci. U. S. A.* **105**(38), 14271–14276 (2008).

54. M. Leutenegger, C. Eggeling, and S. W. Hell, "Analytical description of STED microscopy performance," *Opt. Express* **18**(25), 26417–26429 (2010).
55. K. Y. Han et al., "Three-dimensional stimulated emission depletion microscopy of nitrogen-vacancy centers in diamond using continuous-wave light," *Nano Lett.* **9**(9), 3323–3329 (2009).
56. G. Moneron et al., "Fast STED microscopy with continuous wave fiber lasers," *Opt. Express* **18**(2), 1302–1309 (2010).
57. M. Bouzin et al., "Stimulated emission properties of fluorophores by CW-STED single molecule spectroscopy," *J. Phys. Chem. B* **117**(51), 16405–16415 (2013).
58. C. Kuang, W. Zhao, and G. Wang, "Far-field optical nanoscopy based on continuous wave laser stimulated emission depletion," *Rev. Sci. Instrum.* **81**(5), 053709 (2010).
59. F. Helmchen and W. Denk, "Deep tissue two-photon microscopy," *Nat. Methods* **2**(12), 932–940 (2005).
60. A. Diaspro, G. Chirico, and M. Collini, "Two-photon fluorescence excitation and related techniques in biological microscopy," *Q. Rev. Biophys.* **38**(2), 97–166 (2005).
61. K. Svoboda and R. Yasuda, "Principles of two-photon excitation microscopy and its applications to neuroscience," *Neuron* **50**(6), 823–839 (2006).
62. G. Moneron and S. W. Hell, "Two-photon excitation STED microscopy," *Opt. Express* **17**(17), 14567–14573 (2009).
63. J. B. Ding, K. T. Takasaki, and B. L. Sabatini, "Supraresolution imaging in brain slices using stimulated-emission depletion two-photon laser scanning microscopy," *Neuron* **63**(4), 429–437 (2009).
64. Q. Li, S.S.H. Wu, and K. C. Chou, "Subdiffraction-limit two-photon fluorescence microscopy for GFP-tagged cell imaging," *Biophys. J.* **97**(12), 3224–3228 (2009).
65. T. Scheul et al., "Two-photon excitation and stimulated emission depletion by a single wavelength," *Opt. Express* **19**(19), 18036–18048 (2011).
66. P. Bianchini et al., "Single-wavelength two-photon excitation-stimulated emission depletion (SW2PE-STED) superresolution imaging," *Proc. Natl. Acad. Sci. U. S. A.* **109**(17), 6390–6393 (2012).
67. T. A. Klar et al., "Fluorescence microscopy with diffraction resolution barrier broken by stimulated emission," *Proc. Natl. Acad. Sci.* **97**(15), 8206–8210 (2000).
68. T. J. Gould, J. R. Myers, and J. Bewersdorf, "Total internal reflection STED microscopy," *Opt. Express* **19**(14), 13351–13357 (2011).
69. M. Leutenegger et al., "Fluorescence correlation spectroscopy with a total internal reflection fluorescence STED microscope (TIRF-STED-FCS)," *Opt. Express* **20**(5), 5243–5263 (2012).
70. H. Gugel et al., "Cooperative 4Pi excitation and detection yields seven-fold sharper optical sections in live-cell microscopy," *Biophys. J.* **87**(6), 4146–4152 (2004).
71. R. Schmidt et al., "Spherical nanosized focal spot unravels the interior of cells," *Nat. Methods* **5**(6), 539–544 (2008).
72. P. Bingen et al., "Parallelized STED fluorescence nanoscopy," *Opt. Express* **19**(24), 23716–23726 (2011).
73. A. Chmyrov et al., "Nanoscopy with more than 100,000 'doughnuts,'" *Nat. Methods* **10**(8), 737–740 (2013).
74. A. Gahlmann et al., "Quantitative multicolor subdiffraction imaging of bacterial protein ultrastructures in three dimensions," *Nano Lett.* **13**(3), 987–993 (2013).
75. P. Mahou et al., "Multicolor two-photon tissue imaging by wavelength mixing," *Nat. Methods* **9**(8), 815–818 (2012).
76. S. Abrahamsson et al., "Fast multicolor 3D imaging using aberration-corrected multifocus microscopy," *Nat. Methods* **10**(1), 60–63 (2013).
77. L. Schermelleh et al., "Subdiffraction multicolor imaging of the nuclear periphery with 3D structured illumination microscopy," *Science* **320**(5881), 1332–1336 (2008).
78. S. Wilmes et al., "Triple-color super-resolution imaging of live cells: resolving submicroscopic receptor organization in the plasma membrane," *Angew. Chem. Int. Ed.* **51**(20), 4868–4871 (2012).
79. T. Klein, S. van de Linde, and M. Sauer, "Live-cell super-resolution imaging goes multicolor," *ChemBioChem* **13**(13), 1861–1863 (2012).
80. L. Meyer et al., "Dual-color STED microscopy at 30-nm focal-plane resolution," *Small* **4**(8), 1095–1100 (2008).
81. F. Gottfert et al., "Coaligned dual-channel STED nanoscopy and molecular diffusion analysis at 20 nm resolution," *Biophys. J.* **105**(1), L1–L3 (2013).
82. P. A. Pellett et al., "Two-color STED microscopy in living cells," *Biomed. Opt. Express* **2**(8), 2364–2371 (2011).
83. J. Tønnesen et al., "Two-color STED microscopy of living synapses using a single laser-beam pair," *Biophys. J.* **101**(10), 2545–2552 (2011).
84. K. I. Willig et al., "Dual-label STED nanoscopy of living cells using photochromism," *Nano Lett.* **11**(9), 3970–3973 (2011).
85. J. Buckers et al., "Simultaneous multi-lifetime multi-color STED imaging for colocalization analyses," *Opt. Express* **19**(4), 3130–3143 (2011).
86. G. Vicidomini et al., "Sharper low-power STED nanoscopy by time gating," *Nat. Methods* **8**(7), 571–573 (2011).
87. X. Hao et al., "Manipulation of doughnut focal spot by image inverting interferometry," *Opt. Lett.* **37**(5), 821–823 (2012).
88. M. Fernandez-Suarez and A. Y. Ting, "Fluorescent probes for super-resolution imaging in living cells," *Nat. Rev. Mol. Cell Biol.* **9**(12), 929–943 (2008).
89. C. Grunwald et al., "Quantum-yield-optimized fluorophores for site-specific labeling and super-resolution imaging," *J. Am. Chem. Soc.* **133**(21), 8090–8093 (2011).
90. M. D. Lesoine et al., "Subdiffraction, luminescence-depletion imaging of isolated, giant, CdSe/CdS nanocrystal quantum dots," *J. Phys. Chem. C* **117**(7), 3662–3667 (2013).
91. G. Lukinavicius et al., "Fluorogenic probes for live-cell imaging of the cytoskeleton," *Nat. Methods* **11**(7), 731–733 (2014).
92. V. Westphal et al., "Laser-diode-stimulated emission depletion microscopy," *Appl. Phys. Lett.* **82**(18), 3125–3127 (2003).
93. D. Wildanger et al., "STED microscopy with a supercontinuum laser source," *Opt. Express* **16**(13), 9614–9621 (2008).
94. B. R. Rankin, R. R. Kellner, and S. W. Hell, "Stimulated-emission-depletion microscopy with a multicolor stimulated-Raman-scattering light source," *Opt. Lett.* **33**(21), 2491–2493 (2008).
95. B. Harke et al., "A novel nanoscopic tool by combining AFM with STED microscopy," *Opt. Nanosc.* **1**(1), 1–6 (2012).
96. J. V. Chacko, F. C. Zanacchi, and A. Diaspro, "Probing cytoskeletal structures by coupling optical superresolution and AFM techniques for a correlative approach," *Cytoskeleton* **70**(11), 729–740 (2013).
97. I. Heller et al., "STED nanoscopy combined with optical tweezers reveals protein dynamics on densely covered DNA," *Nat. Methods* **10**(9), 910–U132 (2013).

Bhanu Neupane completed BS and MS degrees from Tribhuvan University, Nepal. He finished his PhD degree in 2011 from Kansas State University. In his PhD research, he used high-resolution spectroscopies to study the energy and electron transfer processes in natural and artificial photosynthetic systems. His current research at North Carolina State University, under the supervision of Profs. Frances Ligler and Gufeng Wang, is related to the understanding of dynamic events in live cells using STED microscopy.

Frances S. Ligler is the Lampe Distinguished Professor of Biomedical Engineering with extensive publications/patents in microfluidics, analytical systems, biomaterials, and 11 commercial biosensor products. She has been elected member and councilor of the National Academy of Engineering. She earned a BS from Furman University and both a DPhil and a DSc from Oxford University. She has an honorary doctorate from the Agricultural University of Athens and is an elected fellow of SPIE, AIMBE, and AAAS.

Gufeng Wang obtained his BS from Nanjing University, China, and his PhD in analytical chemistry from the University of Iowa. He worked as a postdoctoral associate in Iowa State University and Ames Laboratory, U.S. Department of Energy. He is currently an assistant professor in chemistry, North Carolina State University. His research interests include developing super-resolution optical microscopy to study biological problems and mass transport in confined space.